Letter

$\mathcal{PT}$-symmetric non-Hermitian Hopf metal

Seik Pak,[1] Cheol Hun Yeom,[1,2] Sonu Verma,[3,*] and Moon Jip Park[1,†]
[1]*Department of Physics, Hanyang University, Seoul 04763, Republic of Korea*
[2]*Department of Physics, Konkuk University, Seoul 05029, Republic of Korea*
[3]*Center for Theoretical Physics of Complex Systems, Institute for Basic Science, Daejeon 34126, Korea*

(Received 3 November 2023; revised 5 February 2024; accepted 13 February 2024; published 8 March 2024)

The Hopf insulator is a representative class of three-dimensional topological insulators beyond the standard topological classification methods based on K theory. In this Letter, we describe the metallic counterpart of the Hopf insulator in non-Hermitian systems. While the Hopf invariant is not a stable topological index due to the additional non-Hermitian degree of freedom, we show that the $\mathcal{PT}$ symmetry stabilizes the Hopf invariant even in the presence of the non-Hermiticity. In sharp contrast to the Hopf insulator phase in the Hermitian counterpart, we describe an interesting result that the non-Hermitian Hopf bundle exhibits topologically protected non-Hermitian degeneracy, characterized by the two-dimensional surface of exceptional points. Despite the non-Hermiticity, the Hopf metal has the quantized Zak phase, which results in bulk-boundary correspondence by showing drumheadlike surface states at the boundary. Finally, we show that, by breaking $\mathcal{PT}$ symmetry, the nodal surface deforms into knotted exceptional lines. Our description of the Hopf metal phase confirms the existence of the non-Hermitian topological phase outside the framework of the standard topological classifications.

DOI: 10.1103/PhysRevResearch.6.L012053

Introduction. In three-dimensions, the insulating phases with two-band systems are topologically classified by Hopf invariant, where the nontrivial topology is characterized by the eigenspinors with the Hopf bundle structure [1–7]. The Hopf insulator has gathered great interest due to its unusual phenomena. That is, the topological stability only persists when the number of bands is equal to 2. The addition of auxiliary trivial bands trivializes the topological index. This instability features incompatibility of K-theory-based classification methods for the description of the Hopf insulator [8–11]. In this regard, there has been a considerable effort in studying such delicate topological phases both experimentally [12,13] and theoretically [14–17]. As a similar phenomenon but with different physical origins, the fragile topology has also been suggested as an interesting phase that is detectable by the symmetry indicator even with the trivial K-theory index [18–29].

Non-Hermitian systems have emerged as a transformative area to extend the knowledge of topological phases. In general, the complex energy spectra can enrich or nullify the Hermitian topological classifications [30–50]. Meanwhile, in symmetry-protected topological phases, $\mathcal{PT}$ symmetry plays an important role since it ensures either real or complex pairs of eigenenergies. Unlike the Hermitian systems, the transition from real to complex spectrum occurs by passing through the non-Hermitian degeneracy, known as an exceptional point (EP) [51–61]. While K theory is applicable to the topological classification of the EP as well [30], the energy spectrum of the EP exhibits eigenstates coalescence, which shows physical phenomena completely different from the Hermitian systems.

In this work, we describe the Hopf metal phase, the non-Hermitian counterpart of the Hopf insulator. In general, the introduction of the non-Hermiticity can nullify the homotopy classifications of the Hopf bundle. However, we show that the presence of the additional $\mathcal{PT}$ symmetry allows us to define the non-Hermitian Hopf invariant. Unlike the Hopf insulator in the Hermitian phase, the Hopf metal is characterized by the topologically protected two-dimensional surfaces of the EP (exceptional surface), which shows intriguingly different behavior from the Hermitian Hopf insulators. Similarly to the other topological systems protected by the finite homotopy group, the addition of the trivial band destabilizes the Hopf metal phase and the exceptional surfaces. In addition, we show that the Hopf metal phase exhibits bulk-boundary correspondence, where the surface state manifests as the drumhead surface state. The addition of $\mathcal{PT}$ symmetry-breaking perturbation results in the deformation of the exceptional surface into the nodal lines of the exceptional points with nontrivial linking structures. Finally, we discuss the experimental realization of the Hopf metal in various experimental platforms. Our work contributes to the understanding of topological phases of matter by describing the non-Hermitian topological phase protected by the Hopf invariant.

$\mathcal{PT}$-symmetric non-Hermitian system. In Hermitian systems, the Bloch Hamiltonian of a two-band insulator can be represented by the spinor $\vec{n}(\mathbf{k})$ on the Bloch sphere (S^2) as $h_0(\mathbf{k}) = \vec{n}(\mathbf{k}) \cdot \vec{\sigma}$, where $\vec{\sigma}$ is the Pauli matrix representing the sublattice (internal) degree of freedom. When the Chern number vanishes in the two-dimensional subspace of the Brillouin zone (T^3), the Hopf invariant [$w(\vec{n}) \in \mathbb{Z}$]

*sonu.vermaiitk@gmail.com
†moonjippark@hanyang.ac.kr

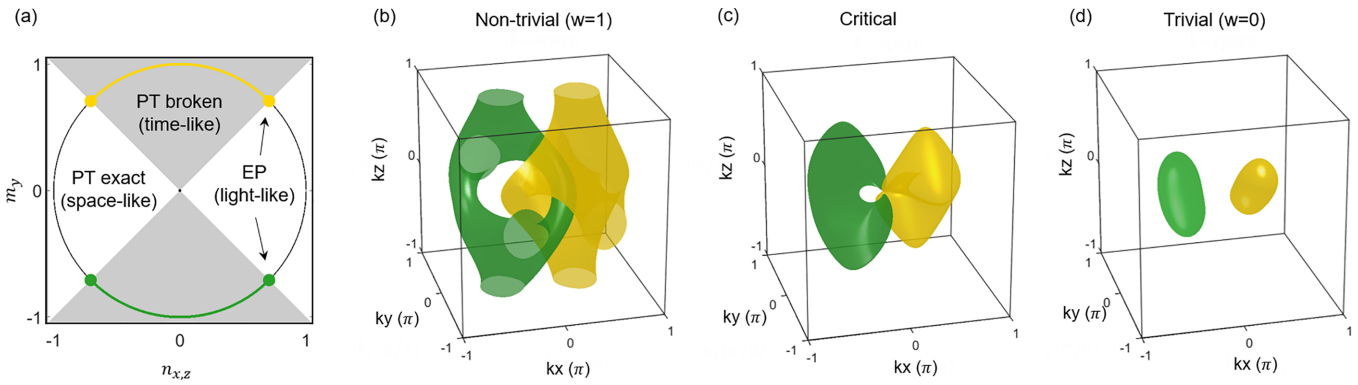

FIG. 1. (a) Illustration of $\mathcal{PT}$-symmetric energy spectra. Grey and white regions indicate timelike and spacelike eigenspinors, where the eigenenergies are purely imaginary and purely real respectively. The boundary between the two regions corresponds to the light cone where the lightlike spinors give rise to the exceptional point (green and yellow dots). (b)–(d) the preimage of the lightlike spinors (EP) in the Brillouin zone for the cases with (b) nontrivial ($w = 1, m = 2$), (c) critical ($m = 3$), and (d) trivial ($w = 0, m = 4$) Hopf invariants. The interior of the exceptional surface corresponds to the lightlike region, while the exterior is the spacelike region. In the nontrivial case, the two exceptional surfaces are linked together. At the critical point, the two exceptional two surfaces intersect. For the trivial case, two nodal surfaces are completely separated. Increasing the value of m further, the surfaces become flatter until they completely disappear.

topologically classifies the two-band insulators [1]. Geometrically, for a given spin $\vec{n}_0$ in the Bloch sphere, a preimage $\mathbf{k}$ in the Brillouin zone (BZ) such that $\vec{n}(\mathbf{k}) = \vec{n}_0$ forms a closed contour. The Hopf invariant counts the linking numbers between the preimages of two different spins. To be explicit, for the spinor configuration $\vec{n}(\mathbf{k}) = \hat{z}^\dagger(\mathbf{k})\vec{\sigma}\hat{z}(\mathbf{k})$, the Hopf invariant can be evaluated as [2]

$$w(n_x(\mathbf{k}), n_y(\mathbf{k}), n_z(\mathbf{k})) = \frac{1}{12\pi^2}\int_{T^3}\frac{d^3k}{|z|^4}\epsilon^{abcd}\epsilon^{ijk}N_a\partial_i N_b\partial_j N_c\partial_k N_d, \quad (1)$$

where $\hat{z}(\mathbf{k})$ is the normalized complex vector $z(\mathbf{k})$, which is given as $z(\mathbf{k}) = (N_1(\mathbf{k}) + iN_2(\mathbf{k}), N_3(\mathbf{k}) + iN_4(\mathbf{k}))^T$. The non zero Hopf invariant characterizes the Hopf insulator. The change in the Hopf invariant can only occur by undergoing gapless transitions.

However, as we introduce the non-Hermiticity, the Hamiltonian can generally contain additional anti-Hermitian components as follows:

$$h(\mathbf{k}) = [n_x(\mathbf{k}) + im_x(\mathbf{k})]\sigma_x + [n_z(\mathbf{k}) + im_z(\mathbf{k})]\sigma_z + [n_y(\mathbf{k}) + im_y(\mathbf{k})]\sigma_y, \quad (2)$$

where $n_i(\mathbf{k})$ $[m_i(\mathbf{k})]$ represent the Hermitian [anti-Hermitian] components. Since the Hamiltonian is now represented by six real parameters [62], the non-Hermiticity can destabilize the Hopf invariant. Nevertheless, the presence of the additional $\mathcal{PT}$ symmetry, $\mathcal{PT}h(\mathbf{k})\mathcal{PT}^{-1} = h(\mathbf{k})^*$ [51], allows us to choose a gauge such that the Hamiltonian can be represented as a real-valued matrix. Accordingly, three of the parameters vanish $[n_y(\mathbf{k}) = m_x(\mathbf{k}) = m_z(\mathbf{k}) = 0]$. The remaining nonzero Hermitian and anti-Hermitian parameters $(n_x(\mathbf{k}), m_y(\mathbf{k}), n_z(\mathbf{k}))$ form a three-component vector that can be projected on S^2. Therefore, the $\mathcal{PT}$-symmetric non-Hermitian system can be classified by the modified Hopf invariant, $w(n_x(\mathbf{k}), m_y(\mathbf{k}), n_z(\mathbf{k}))$, which is well-defined except for transition point characterized by the null Hamiltonian $h(\mathbf{k}) = 0$.

In the complex energy plane, the energy dispersion of Eq. (2) is generally complex valued, and is given as

$$E(\mathbf{k}) = \pm\sqrt{|\mathbf{n}(\mathbf{k})|^2 - |\mathbf{m}(\mathbf{k})|^2 + 2i\mathbf{n}(\mathbf{k})\cdot\mathbf{m}(\mathbf{k})}. \quad (3)$$

The presence of $\mathcal{PT}$ symmetry ensures that the Hermitian and anti-Hermitian vectors are perpendicular to each other, $\vec{n}(\mathbf{k}) \perp \vec{m}(\mathbf{k})$. The corresponding energy eigenvalues are confined to either real ($\mathcal{PT}$-exact) or imaginary ($\mathcal{PT}$-broken) axes. Depending on the spectral property, the BZ can be classified into two distinct regions: spacelike and timelike regions. The momenta with *spacelike* spinors $[n_x^2(\mathbf{k}) + n_z^2(\mathbf{k}) - m_y^2(\mathbf{k}) > 0]$ and *timelike* spinors $[n_x^2(\mathbf{k}) + n_z^2(\mathbf{k}) - m_y^2(\mathbf{k}) < 0]$ correspond to the $\mathcal{PT}$-exact and $\mathcal{PT}$-broken phases respectively [51]. The boundary between the two region is described by a *lightlike* spinor $[n_x^2(\mathbf{k}) + n_z^2(\mathbf{k}) - m_y^2(\mathbf{k}) = 0]$ that exhibit the EP. On the Bloch sphere, the lightlike spinors are composed of two separable rings of the future and past light cones [see Fig. 1(a)].

Three-dimensional Hopf metal. To exemplify the three-dimensional non-Hermitian Hopf bundle, we consider the three-component vector $(n_x(\mathbf{k}), m_y(\mathbf{k}), n_z(\mathbf{k}))$. with the dispersion given as $N_1(\mathbf{k}) = \sin(k_x)$, $N_2(\mathbf{k}) = \sin(k_y)$, $N_3(\mathbf{k}) = \sin(k_z)$, and $N_4(\mathbf{k}) = m - \cos(k_x) - \cos(k_y) - \cos(k_z)$. The Hopf invariant w has a nontrivial value of $+1$ (-2) when $1 < |m| < 3$ $(-1 < m < 1)$. Otherwise, it has trivial value [3]. Figures 1(b)–1(d) show the exemplified exceptional surfaces (green and yellow surfaces) with the non-trivial Hopf invariant, topological phase transition, and the trivial phase respectively. The interior and the exterior of the exceptional surfaces correspond to the timelike and the spacelike regions respectively. The nontrivial Hopf invariant $[\omega(n_x, m_y, n_z) \neq 0]$ ensures that there exists a nonempty preimage in the BZ for any point in S^2. Due to the nonzero Hopf invariant, the preimage of the future and past lightlike spinors manifests as the two intertwined surfaces of the exceptional point (exceptional surface) [Fig. 1(b)]. The intertwined structure topologically protects the exceptional surfaces from shrinking and vanishing. As a result, the nontrivial Hopf invariant manifests as the

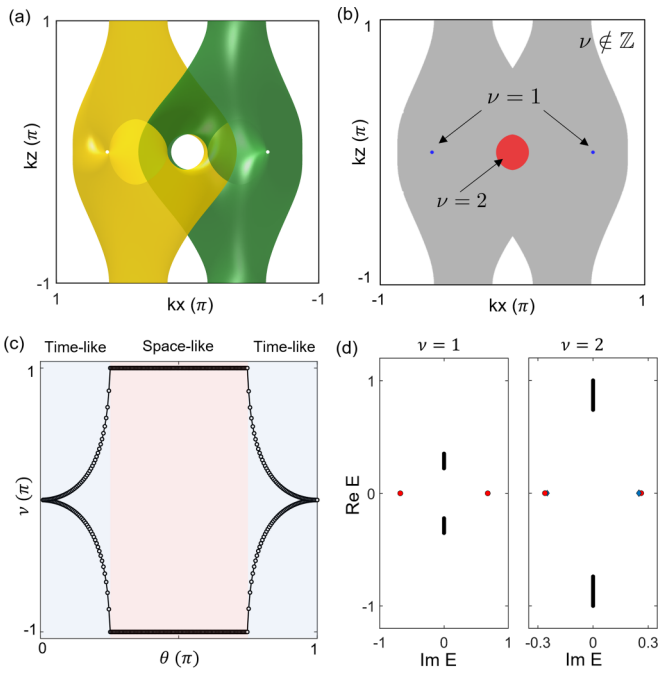

FIG. 2. (a) Projected three-dimensional Hopf metal on the k_x-k_z plane. (b) Illustration of the Zak phase integrated along the k_y direction. Red and blue regions have nontrivial Zak phases 2π ($\nu = 2$) and π ($\nu = 1$). The grey region has an ill-defined Zak phase since the line of the integration passes through the exceptional surface. (c) Zak phases calculated over a loop on the Bloch sphere, where the polar angle θ is defined as the angle between spinor and m_y axis. A loop of the spacelike region with a winding number has a quantized Zak phase of π regardless of the presence of the non-Hermitian term. The Zak phase of a loop on a timelike region loses its quantization. (d) The eigenenergy spectra in the open boundary condition. Red and blue dots indicate the topological boundary modes, while the black dots represent the bulk spectra. For $\nu = 1$ and $\nu = 2$ loops, (k_x, k_z) are set to $(0.31\pi, 0)$ and $(0.03\pi, 0.03\pi)$, corresponding to blue and red regions in (b), respectively.

topologically protected two-dimensional surface of the exceptional point, which we refer to as the *Hopf metal* phase. In the case of the trivial Hopf invariant [Fig. 1(d)], we still find the exceptional surfaces. However, these surfaces are accidental, since they can be self-annihilated by adiabatic deformation.

Bulk-boundary correspondence. The exceptional surface divides the BZ into spacelike and timelike regions. We can consider one-dimensional lines of the gapped regions to define the Zak phase [63,64] [For example, see red and blue regions in Fig. 2(b)]. In general, unlike the Hermitian systems, the presence of $\mathcal{PT}$ symmetry alone does not guarantee the quantization of the Zak phase. Nevertheless, we explicitly show that the Wilson loop of the spacelike region still retains the quantization of the Zak phase [see Fig. 2(c)], while the Zak phase in the timelike region loses its quantization. (See Supplemental Material for a detailed proof [65].) On the Bloch sphere, the quantization of the Zak phase corresponds to the winding number of the loop of the spinor around the north pole. Any loop of spacelike spinor has a well-defined winding number since the winding number cannot change without passing through lightlike regions (EP). On the other hand, any loop of a timelike spinor can adiabatically deform and therefore vanish.

As a result, we can define a quantized Zak phase ($\nu \in \mathbb{Z}$) on the exterior of the exceptional surface [red and blue regions in Fig. 2(b)]. Along the one-dimensional line outside the exceptional surface, the $\mathbb{Z}$-valued Zak phase can be defined as

$$\nu = \frac{1}{i\pi} \log \det\left[P \exp\left(\oint \mathcal{A}(\mathbf{k}) \cdot d\mathbf{k}\right)\right], \tag{4}$$

where $\mathcal{A}(\mathbf{k}) = i\langle n_R(\mathbf{k})|\partial_{\mathbf{k}}|n_R(\mathbf{k})\rangle$ is the non-Hermitian Berry connection. $|n_R(\mathbf{k})\rangle$ is the right eigenstate at the momentum $\mathbf{k}$. P indicates the path ordering in the contour integration. Here, the Zak phase is rather more $\mathbb{Z}$ valued than $\mathbb{Z}_2$ since we consider the two-band model. The physical manifestation of the nontrivial Zak phase is 2ν number of the topological boundary modes within the line gap in the complex energy plane [Fig. 2(d)]. In three-dimensional systems with the open boundary condition along y direction, the boundary modes manifest as a drumheadlike topological surface state. The drumhead surface extends as a function of k_x and k_z until the Wilson line touches the bulk exceptional surfaces [grey region in Fig. 2(b)].

$\mathcal{PT}$-symmetry broken phases. We consider the effect of the $\mathcal{PT}$-symmetry breaking perturbation. Due to the perturbation, the energy spectra can attain an arbitrary complex phase [see Fig. 3(a)]. Accordingly, the exceptional surface loses topological protection. Nevertheless, the exceptional surface can deform into the topologically protected line of the EP (exceptional line) rather than the immediate line gap opening. The exceptional line has a closed line gap, and it is protected by the point gap topology (A class in non-Hermitian Altland-Zirnbauer classification [30]). We can define the vorticity ($2W \in \mathbb{Z}$) of the complex eigenvalues as

$$W(E_{\pm}(\mathbf{k})) = \frac{1}{2\pi i} \oint d\mathbf{k} \cdot \frac{d}{d\mathbf{k}} \log \det[E_{\pm}(\mathbf{k})]. \tag{5}$$

Here, the integration is performed over the loop that encircles the exceptional line. $E_{\pm}(\mathbf{k})$ is the complex eigenenergy. The integer-valued vorticity counts the number of the eigenenergy encircling ($W = 2N$, $N \in \mathbb{Z}$) around the origin in the complex energy plane. The half integer-valued vorticity ($W = 2N + 1$) can also occur by having the eigenstate switching effect [66,67].

To explicitly show the formation of the exceptional line, we consider the additional anti- $\mathcal{PT}$-symmetric perturbation as $V = i\lambda_x\sigma_x + i\lambda_z\sigma_z + \lambda_y\sigma_y$, where $\lambda_{x,y,z}$ are small real parameters. The corresponding perturbed energy eigenvalues are given as $E(\mathbf{k}) = \pm[|n(\mathbf{k})|^2 - |m(\mathbf{k})|^2 - (\lambda_x^2 + \lambda_z^2 - \lambda_y^2) + 2i(\lambda_x n_x + \lambda_y m_y + \lambda_z n_z)]^{\frac{1}{2}}$. Then, the locations of the EP as a function of (n_x, m_y, n_z) are determined by the intersections of the three surfaces, (i) sphere: $n_x^2 + m_y^2 + n_z^2 = 1$; (ii) hyperboloid $n_x^2 + n_z^2 - m_y^2 - (\lambda_x^2 + \lambda_z^2 - \lambda_y^2) = 0$; (iii) plane $\lambda_x n_x + \lambda_y m_y + \lambda_z n_z = 0$. The intersection between the hyperboloid and sphere corresponds to the circles of the lightlike spinors. As the intersection of the circles with the plane deforms the circles into four distinct points, the preimage of these four points manifests as the quartet of the exceptional lines. Figure 3(c) shows examples of the exceptional lines with $W = \pm 1/2$. The exceptional lines are linked to each other as a reminder of the non-trivial Hopf invariant. We note

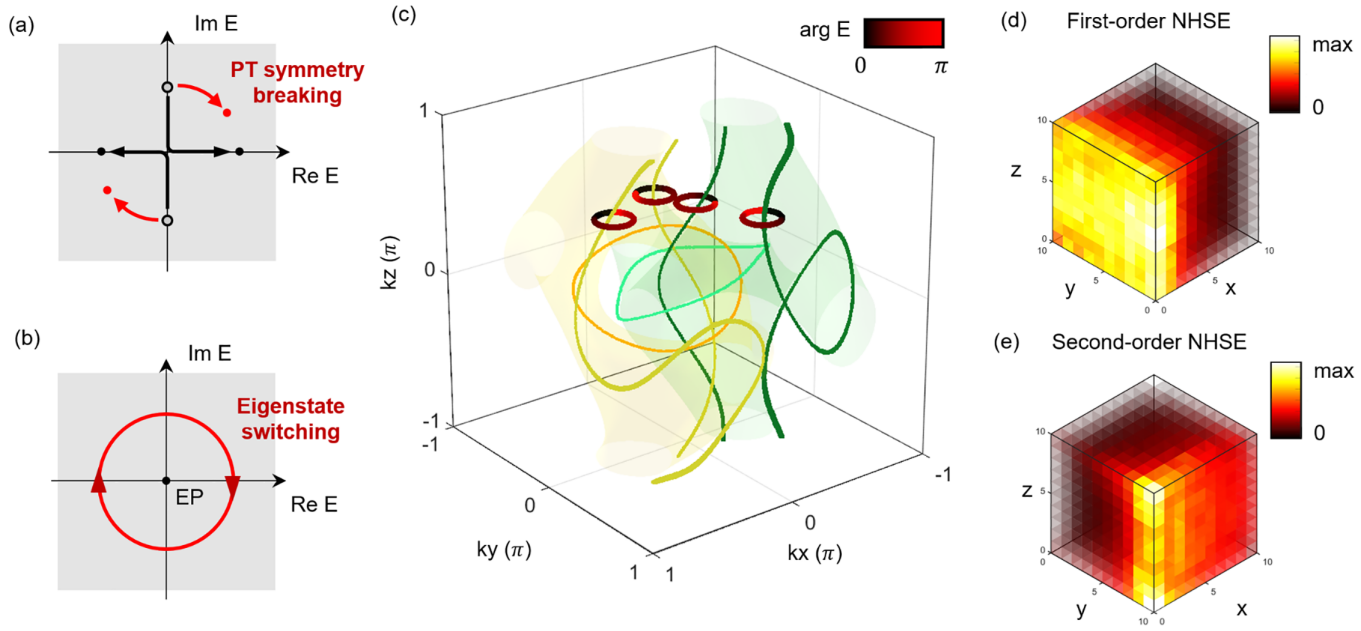

FIG. 3. (a)–(b) Illustration of $\mathcal{PT}$-symmetry breaking perturbation. The presence of the perturbation results in the complex energy spectra. We can define the winding number of the complex energy as a topological invariant. (c) Deformation of the exceptional surface to exceptional nodal lines due to the $\mathcal{PT}$-symmetry-breaking perturbation. Four differently colored lines correspond to four distinct exceptional points. The deformed nodal lines are topologically protected by the winding of the complex energy. (d)–(e) Real-space wave functions in the open boundary conditions. By varying the symmetry-breaking perturbation, the first-order and second-order non-Hermitian skin effects are observed due to the finite spectral area in the complex energy plane.

that the linked structure of the exceptional lines was previously proposed as knotted non-Hermitian metal [68]. Hopf metal corresponds to the $\mathcal{PT}$-symmetric point of the knotted non-Hermitian metal phase.

The finite spectral area due to the winding number manifests as the non-Hermitian skin effect (NHSE) in real space with the open boundary condition [Figs. 3(d) and 3(e)] [69–71]. The charge accumulation of the skin state generally occurs in one of the boundary surfaces (first-order skin effect) [Fig. 3(d)]. As anticipated by Zhang *et al.* [71], the control of the symmetry breaking orientation λ can induce the non-Hermitian skin effect that is dependent on the geometry of the system. By varying symmetry-breaking orientations, we also observe that the higher-order skin effect can be induced where the charge accumulations occur at the one-dimensional hinges [Fig. 3(e)].

Discussions. In this work, we have described the Hopf metal phase protected by the Hopf invariant in non-Hermitian $\mathcal{PT}$-symmetric systems. The topologically protected exceptional surface serves as a hallmark of the Hopf metal, and it features a direct contrast to the Hopf insulator phase in Hermitian systems. It has been known that the realization of the Hopf insulator requires long-range couplings in real space. The experimental realization of the non-Hermitian Hopf metal also demands such long-range coupling. The recent completion of the Hopf insulator in an electric circuit platform is promising, as it can enable efficient design of the model Hamiltonian in addition to the non-Hermitian circuit components [12]. The Hopf insulator has been also proposed in other physical platforms such as a quantum simulator [72] and interacting spin systems [73,74]. We also point out that both of these platforms can effectively engineer the nonreciprocal coupling [75,76], which promises a possible realization of the non-Hermitian Hopf metal phase.

Finally, the implementation of complex momentum dependence in the physical system might be challenging. We find that the non-Hermitian Hopf metal phase persists even though m_y is replaced by a small constant. The linked exceptional surfaces and quantization of the Zak phase are confirmed (see Supplemental Material [65] for details). This approach may offer a more feasible path to experimental implementation due to the reduced complexity in the momentum dependence of the non-Hermitian term.

Acknowledgments. This work was supported by the National Research Foundation of Korea (NRF) funded by the Korea government (MSIT) (Grants No. RS-2023-00252085 and No. RS-2023-00218998). S.V. and M.J.P. acknowledge financial support from the Institute for Basic Science in the Republic of Korea through the Project No. IBS-R024-D1.

[1] J. E. Moore, Y. Ran, and X.-G. Wen, Topological surface states in three-dimensional magnetic insulators, Phys. Rev. Lett. **101**, 186805 (2008).

[2] C. Liu, F. Vafa, and C. Xu, Symmetry-protected topological Hopf insulator and its generalizations, Phys. Rev. B **95**, 161116(R) (2017).

[3] D.-L. Deng, S.-T. Wang, C. Shen, and L.-M. Duan, Hopf insulators and their topologically protected surface states, Phys. Rev. B **88**, 201105(R) (2013).

[4] T. Schuster, S. Gazit, J. E. Moore, and N. Y. Yao, Floquet Hopf insulators, Phys. Rev. Lett. **123**, 266803 (2019).

[5] B. Lapierre, T. Neupert, and L. Trifunovic, N-band Hopf insulator, Phys. Rev. Res. **3**, 033045 (2021).

[6] F. N. Ünal, A. Eckardt, and R.-J. Slager, Hopf characterization of two-dimensional floquet topological insulators, Phys. Rev. Res. **1**, 022003(R) (2019).

[7] A. Graf and F. Piéchon, Massless multifold Hopf semimetals, Phys. Rev. B **108**, 115105 (2023).

[8] C.-K. Chiu, J. C. Y. Teo, A. P. Schnyder, and S. Ryu, Classification of topological quantum matter with symmetries, Rev. Mod. Phys. **88**, 035005 (2016).

[9] S. Ryu, A. P. Schnyder, A. Furusaki, and A. W. W. Ludwig, Topological insulators and superconductors: Tenfold way and dimensional hierarchy, New J. Phys. **12**, 065010 (2010).

[10] A. P. Schnyder, S. Ryu, A. Furusaki, and A. W. W. Ludwig, Classification of topological insulators and superconductors in three spatial dimensions, Phys. Rev. B **78**, 195125 (2008).

[11] A. Kitaev, Periodic table for topological insulators and superconductors, AIP Conf. Proc. **1134**, 22 (2009).

[12] Z. Wang, X.-T. Zeng, Y. Biao, Z. Yan, and R. Yu, Realization of a Hopf insulator in circuit systems, Phys. Rev. Lett. **130**, 057201 (2023).

[13] Y. Kim, H. C. Park, M. Kyung, K. Lee, J.-W. Ryu, O. You, S. Zhang, B. Min, and M. J. Park, Realization of non-Hermitian Hopf bundle matter, Commun. Phys. **6**, 273 (2023).

[14] A. Nelson, T. Neupert, A. Alexandradinata, and T. Bzdušek, Delicate topology protected by rotation symmetry: Crystalline Hopf insulators and beyond, Phys. Rev. B **106**, 075124 (2022).

[15] A. Nelson, T. Neupert, T. Bzdušek, and A. Alexandradinata, Multicellularity of delicate topological insulators, Phys. Rev. Lett. **126**, 216404 (2021).

[16] P. Zhu, A. Alexandradinata, and T. L. Hughes, $\mathbb{Z}_2$ spin Hopf insulator: Helical hinge states and returning thouless pump, Phys. Rev. B **107**, 115159 (2023).

[17] P. Zhu and R.-X. Zhang, Delicate topology of Luttinger semimetal, arXiv:2308.05793

[18] H. C. Po, H. Watanabe, and A. Vishwanath, Fragile topology and Wannier obstructions, Phys. Rev. Lett. **121**, 126402 (2018).

[19] Z.-D. Song, L. Elcoro, and B. A. Bernevig, Twisted bulk-boundary correspondence of fragile topology, Science **367**, 794 (2020).

[20] A. Bouhon, T. Bzdušek, and R.-J. Slager, Geometric approach to fragile topology beyond symmetry indicators, Phys. Rev. B **102**, 115135 (2020).

[21] B. Lian, F. Xie, and B. A. Bernevig, Landau level of fragile topology, Phys. Rev. B **102**, 041402(R) (2020).

[22] M. B. de Paz, M. G. Vergniory, D. Bercioux, A. García-Etxarri, and B. Bradlyn, Engineering fragile topology in photonic crystals: Topological quantum chemistry of light, Phys. Rev. Res. **1**, 032005(R) (2019).

[23] Y. Hwang, J. Ahn, and B.-J. Yang, Fragile topology protected by inversion symmetry: Diagnosis, bulk-boundary correspondence, and Wilson loop, Phys. Rev. B **100**, 205126 (2019).

[24] H. C. Po, L. Zou, T. Senthil, and A. Vishwanath, Faithful tight-binding models and fragile topology of magic-angle bilayer graphene, Phys. Rev. B **99**, 195455 (2019).

[25] B. Bradlyn, Z. Wang, J. Cano, and B. A. Bernevig, Disconnected elementary band representations, fragile topology, and wilson loops as topological indices: An example on the triangular lattice, Phys. Rev. B **99**, 045140 (2019).

[26] H.-X. Wang, G.-Y. Guo, and J.-H. Jiang, Band topology in classical waves: Wilson-loop approach to topological numbers and fragile topology, New J. Phys. **21**, 093029 (2019).

[27] V. Peri, Z.-D. Song, M. Serra-Garcia, P. Engeler, R. Queiroz, X. Huang, W. Deng, Z. Liu, B. A. Bernevig, and S. D. Huber, Experimental characterization of fragile topology in an acoustic metamaterial, Science **367**, 797 (2020).

[28] A. Bouhon, A. M. Black-Schaffer, and R.-J. Slager, Wilson loop approach to fragile topology of split elementary band representations and topological crystalline insulators with time-reversal symmetry, Phys. Rev. B **100**, 195135 (2019).

[29] F. N. Ünal, A. Bouhon, and R.-J. Slager, Topological euler class as a dynamical observable in optical lattices, Phys. Rev. Lett. **125**, 053601 (2020).

[30] K. Kawabata, K. Shiozaki, M. Ueda, and M. Sato, Symmetry and topology in non-Hermitian physics, Phys. Rev. X **9**, 041015 (2019).

[31] M. R. Hirsbrunner, T. M. Philip, and M. J. Gilbert, Topology and observables of the non-Hermitian Chern insulator, Phys. Rev. B **100**, 081104(R) (2019).

[32] A. Ghatak and T. Das, New topological invariants in non-Hermitian systems, J. Phys.: Condens. Matter **31**, 263001 (2019).

[33] K. Esaki, M. Sato, K. Hasebe, and M. Kohmoto, Edge states and topological phases in non-Hermitian systems, Phys. Rev. B **84**, 205128 (2011).

[34] F. K. Kunst, E. Edvardsson, J. C. Budich, and E. J. Bergholtz, Biorthogonal bulk-boundary correspondence in non-Hermitian systems, Phys. Rev. Lett. **121**, 026808 (2018).

[35] F. Song, S. Yao, and Z. Wang, Non-Hermitian topological invariants in real space, Phys. Rev. Lett. **123**, 246801 (2019).

[36] Z. Yang and J. Hu, Non-Hermitian Hopf-link exceptional line semimetals, Phys. Rev. B **99**, 081102(R) (2019).

[37] S. Yao and Z. Wang, Edge states and topological invariants of non-Hermitian systems, Phys. Rev. Lett. **121**, 086803 (2018).

[38] S. Yao, F. Song, and Z. Wang, Non-Hermitian Chern bands, Phys. Rev. Lett. **121**, 136802 (2018).

[39] Z. Gong, Y. Ashida, K. Kawabata, K. Takasan, S. Higashikawa, and M. Ueda, Topological phases of non-Hermitian systems, Phys. Rev. X **8**, 031079 (2018).

[40] D. S. Borgnia, A. J. Kruchkov, and R.-J. Slager, Non-Hermitian boundary modes and topology, Phys. Rev. Lett. **124**, 056802 (2020).

[41] E. J. Bergholtz, J. C. Budich, and F. K. Kunst, Exceptional topology of non-Hermitian systems, Rev. Mod. Phys. **93**, 015005 (2021).

[42] J. M. Zeuner, M. C. Rechtsman, Y. Plotnik, Y. Lumer, S. Nolte, M. S. Rudner, M. Segev, and A. Szameit, Observation of a topological transition in the bulk of a non-Hermitian system, Phys. Rev. Lett. **115**, 040402 (2015).

[43] K. Yokomizo and S. Murakami, Non-Bloch band theory of non-Hermitian systems, Phys. Rev. Lett. **123**, 066404 (2019).

[44] J. L. K. König, K. Yang, J. C. Budich, and E. J. Bergholtz, Braid-protected topological band structures with unpaired exceptional points, Phys. Rev. Res. **5**, L042010 (2023).

[45] Z. Li and R. S. K. Mong, Homotopical characterization of non-Hermitian band structures, Phys. Rev. B **103**, 155129 (2021).
[46] C. C. Wojcik, X.-Q. Sun, T. Bzdušek, and S. Fan, Homotopy characterization of non-Hermitian Hamiltonians, Phys. Rev. B **101**, 205417 (2020).
[47] V. M. Martinez Alvarez, J. E. Barrios Vargas, and L. E. F. Foa Torres, Non-Hermitian robust edge states in one dimension: Anomalous localization and eigenspace condensation at exceptional points, Phys. Rev. B **97**, 121401(R) (2018).
[48] J. Zhong, C. C. Wojcik, D. Cheng, and S. Fan, Numerical and theoretical study of eigenenergy braids in two-dimensional photonic crystals, Phys. Rev. B **108**, 195413 (2023).
[49] Y. S. S. Patil, J. Höller, P. A. Henry, C. Guria, Y. Zhang, L. Jiang, N. Kralj, N. Read, and J. G. E. Harris, Measuring the knot of non-Hermitian degeneracies and non-commuting braids, Nature (London) **607**, 271 (2022).
[50] K. Yang, Z. Li, J. L. K. König, L. Rødland, M. Stålhammar, and E. J. Bergholtz, Homotopy, symmetry, and non-Hermitian band topology, arXiv:2309.14416.
[51] C. M. Bender and P. D. Mannheim, $\mathcal{PT}$ symmetry and necessary and sufficient conditions for the reality of energy eigenvalues, Phys. Lett. A **374**, 1616 (2010).
[52] R. El-Ganainy, K. G. Makris, M. Khajavikhan, Z. H. Musslimani, S. Rotter, and D. N. Christodoulides, Non-Hermitian physics and $\mathcal{PT}$ symmetry, Nat. Phys. **14**, 11 (2018).
[53] X.-L. Zhang, T. Jiang, and C. T. Chan, Dynamically encircling an exceptional point in anti-parity-time symmetric systems: asymmetric mode switching for symmetry-broken modes, Light Sci. Appl. **8**, 88 (2019).
[54] M. Sakhdari, M. Hajizadegan, Q. Zhong, D. N. Christodoulides, R. El-Ganainy, and P.-Y. Chen, Experimental observation of $\mathcal{PT}$ symmetry breaking near divergent exceptional points, Phys. Rev. Lett. **123**, 193901 (2019).
[55] Ş. K. Özdemir, S. Rotter, F. Nori, and L. Yang, Parity–time symmetry and exceptional points in photonics, Nat. Mater. **18**, 783 (2019).
[56] H. Ramezani, T. Kottos, V. Kovanis, and D. N. Christodoulides, Exceptional-point dynamics in photonic honeycomb lattices with $\mathcal{PT}$ symmetry, Phys. Rev. A **85**, 013818 (2012).
[57] Z. G. Yuto Ashida and M. Ueda, Non-Hermitian physics, Adv. Phys. **69**, 249 (2020).
[58] I. Mandal and E. J. Bergholtz, Symmetry and higher-order exceptional points, Phys. Rev. Lett. **127**, 186601 (2021).
[59] Y. Choi, C. Hahn, J. W. Yoon, and S. H. Song, Observation of an anti-pt-symmetric exceptional point and energy-difference conserving dynamics in electrical circuit resonators, Nat. Commun. **9**, 2182 (2018).
[60] K. Ding, Z. Q. Zhang, and C. T. Chan, Coalescence of exceptional points and phase diagrams for one-dimensional $\mathcal{PT}$-symmetric photonic crystals, Phys. Rev. B **92**, 235310 (2015).
[61] H. Zhou, J. Y. Lee, S. Liu, and B. Zhen, Exceptional surfaces in $\mathcal{PT}$-symmetric non-Hermitian photonic systems, Optica **6**, 190 (2019).
[62] Here, we ignore the component of the identity matrix since it only shifts the overall energy.
[63] J. C. Y. Teo and C. L. Kane, Topological defects and gapless modes in insulators and superconductors, Phys. Rev. B **82**, 115120 (2010).
[64] K. Kawabata, T. Bessho, and M. Sato, Classification of exceptional points and non-Hermitian topological semimetals, Phys. Rev. Lett. **123**, 066405 (2019).
[65] See Supplemental Material at http://link.aps.org/supplemental/10.1103/PhysRevResearch.6.L012053 for a deltailed proof or the quantization of the Zak phase in space like region.
[66] W. D. Heiss, Phases of wave functions and level repulsion, Eur. Phys. J. D **7**, 1 (1999).
[67] W. D. Heiss and A. L. Sannino, Avoided level crossing and exceptional points, J. Phys. A: Math. Gen. **23**, 1167 (1990).
[68] J. Carlström, M. Stålhammar, J. C. Budich, and E. J. Bergholtz, Knotted non-Hermitian metals, Phys. Rev. B **99**, 161115(R) (2019).
[69] N. Okuma, K. Kawabata, K. Shiozaki, and M. Sato, Topological origin of non-Hermitian skin effects, Phys. Rev. Lett. **124**, 086801 (2020).
[70] K. Zhang, Z. Yang, and C. Fang, Correspondence between winding numbers and skin modes in non-Hermitian systems, Phys. Rev. Lett. **125**, 126402 (2020).
[71] K. Zhang, Z. Yang, and C. Fang, Universal non-Hermitian skin effect in two and higher dimensions, Nat. Commun. **13**, 2496 (2022).
[72] X.-X. Yuan, L. He, S.-T. Wang, D.-L. Deng, F. Wang, W.-Q. Lian, X. Wang, C.-H. Zhang, H.-L. Zhang, X.-Y. Chang, and L.-M. Duan, Observation of topological links associated with Hopf insulators in a solid-state quantum simulator, Chin. Phys. Lett. **34**, 060302 (2017).
[73] T. Schuster, F. Flicker, M. Li, S. Kotochigova, J. E. Moore, J. Ye, and N. Y. Yao, Realizing Hopf insulators in dipolar spin systems, Phys. Rev. Lett. **127**, 015301 (2021).
[74] T. Schuster, F. Flicker, M. Li, S. Kotochigova, J. E. Moore, J. Ye, and N. Y. Yao, Floquet engineering ultracold polar molecules to simulate topological insulators, Phys. Rev. A **103**, 063322 (2021).
[75] W. Zhang, X. Ouyang, X. Huang, X. Wang, H. Zhang, Y. Yu, X. Chang, Y. Liu, D.-L. Deng, and L.-M. Duan, Observation of non-Hermitian topology with nonunitary dynamics of solid-state spins, Phys. Rev. Lett. **127**, 090501 (2021).
[76] M.-M. Cao, K. Li, W.-D. Zhao, W.-X. Guo, B.-X. Qi, X.-Y. Chang, Z.-C. Zhou, Y. Xu, and L.-M. Duan, Probing complex-energy topology via non-Hermitian absorption spectroscopy in a trapped ion simulator, Phys. Rev. Lett. **130**, 163001 (2023).